Fuel 225 (2018) 632–645

Contents lists available at ScienceDirect

Fuel

journal homepage: www.elsevier.com/locate/fuel

Full Length Article

Evaluating the effect of ion source gas (N_2, He, and synthetic air) on the ionization of hydrocarbon, condensed aromatic standards, and paraffin fractions by APCI(+)FT-ICR MS

Lindamara M. Souza[a], Lilian V. Tose[a], Felipe Mauro R. Cardoso[b], Felipe P. Fleming[b], Fernanda E. Pinto[a], Ricardo M. Kuster[a], Paulo R. Filgueiras[a], Boniek G. Vaz[c], Wanderson Romão[a,d,*]

[a] Petroleomic and Forensic Chemistry Laboratory, Department of Chemistry, Federal University of Espírito Santo, 29075-910 Vitória, ES, Brazil
[b] Petróleo Brasileiro S/A – PETROBRAS, CENPES, Rio de Janeiro, RJ, Brazil
[c] Chemistry Institute, Federal University of Goiás, 74001-970 Goiânia, GO, Brazil
[d] Federal Institute of Education, Science and Technology of Espírito Santo, 29106-010 Vila Velha, ES, Brazil

GRAPHICAL ABSTRACT

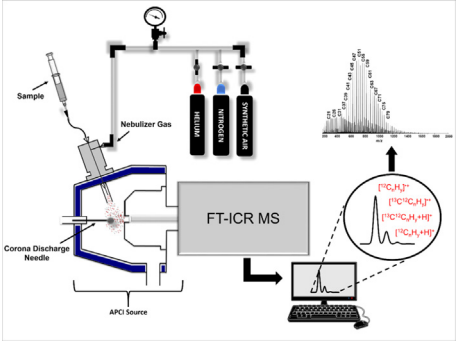

ARTICLE INFO

Keywords:
FT-ICR mass spectrometry
APCI
Hydrocarbon
Paraffin
Ion source gas

ABSTRACT

This study aimed to use different types of ion source gases [synthetic air, nitrogen (N_2), and helium (He)] to compare the ionization efficiency of linear, branched, and cyclic hydrocarbon (HC) standards (i.e., hexatriacontane, squalene, and 5-α-cholestane, respectively), condensed aromatics (CA) standards (i.e., coronene, benz[a]anthracene, and n,n′-bis(3-pentyl)perylene-3,4,9,10-bis(dicarboximide)), one *n*-paraffin standard, containing carbon numbers ranging from C_5 to C_{120}, and two saturated HC fractions. In all cases, a positive-ion mode atmospheric pressure chemical ionization coupled to a Fourier transform ion cyclotron resonance mass spectrometer was used. Isooctane reagent was used to facilitate the ionization of *n*-paraffins. Three ionization mechanisms were observed: electron transfer ($[M]^{rad+}$), proton transfer ($[M+H]^+$), and hydride abstraction ($[M-H]^+$). For the ionization of HC standards, synthetic air and He gases presented better ionization efficiency and produced mass spectra with greater mass accuracy and signal-to-noise rate. Moreover, linear HCs were preferentially ionized through hydride abstraction (production of $[M-H]^+$ ions), whereas the ionization of unsaturated and cyclic HCs mostly occurred through the production of $[M+H]^+$ and $[M^{rad+}]$ species. The unique exception is related to 5-α-cholestane, which is ionized as $[M-H]^+$ in the presence of synthetic air. For the CA standards, N_2 and synthetic air promoted the detection of CA standards mainly by electron transfer

* Corresponding author at: Petroleomic and Forensic Chemistry Laboratory, Department of Chemistry, Federal University of Espírito Santo, 29075-910 Vitória, ES, Brazil.
E-mail address: wandersonromao@gmail.com (W. Romão).

https://doi.org/10.1016/j.fuel.2018.03.180
Received 13 January 2018; Received in revised form 23 March 2018; Accepted 28 March 2018
Available online 10 April 2018
0016-2361/

mechanism, $[M]^{rad+}$ species. Conversely, He favored the proton transfer ionization ($[M+H]^+$) with minimal fragmentation or oxidation of the analyte. In all cases, synthetic air provided mass spectra with excellent signal-to-noise ratio. This performance was attributed to the high reactive-ionizing power of O_2 gas over the HC and CA molecules. For the *n*-paraffin samples, synthetic air and He provided better ionization performance through hydride abstraction ($[M-H]^+$). N_2 favored the production and ionization of heteroatomic compound classes (O_x and NO_x).

1. Introduction

Fourier transform ion cyclotron resonance mass spectrometer (FT-ICR MS) is a mass analyzer with ultra-high-resolution power and mass accuracy [1–4]. FT-ICR MS can be applied to complex matrices, such as petroleum and its fractions [1–4]. Among the data supplied by FT-ICR MS analysis are the elemental composition ($C_cH_hN_nO_oS_s$) and isotopologue profile, which ensure the identification mainly of heteroatoms species [5–7], double-bond equivalent (DBE), which describes the aromaticity of the molecules, and average molecular weight distribution (M_w).

Comisarow and Marshall published one of the earliest works on the application of FT-ICR MS to petroleomics [8]. which was a milestone in the promising progress of this technique. Different sources of ionization can be coupled to the instrument to increase the number of organic compounds and mixtures that can be analyzed. In petroleomics, the following ionization sources are highlighted in the literature: matrix-assisted laser desorption/ionization (MALDI) [9,10], electrospray ionization (ESI) [11–13], atmospheric pressure chemical ionization (APCI) [14,15], atmospheric pressure photoionization (APPI) [16,17], and other derivative sources such as laser-induced acoustic desorption ionization (LIAD) [18,19] and desorption electrospray ionization [20]. Among them, the APCI, MALDI, and LIAD are the main ionization sources used for paraffin analysis [9,14,19]. Hydrocarbons are involved in the deposition process. The characterization of the paraffinic fraction of the oil by FT-ICR MS analysis can reveal differences with respect to population of hydrocarbon molecules, enabling the crude oil industry to comprehend the composition and the chemical structure of paraffins [14].

In 1977, Houriet et al. [21] published a study on the chemical ionization mechanism of *n*-paraffins (*n*-hexane) using methane as the reagent gas applied to FT-ICR MS. In the following years, other studies were also reported. Campbell et al. [22] studied the ionization of paraffins by applying LIAD FT-ICR MS combined with chemical ionization by the cyclopentadienyl cobalt radical ($CpCo^{\cdot+}$). Single pseudomolecular ions were produced from HCs ($C_{24}H_{50}$ to $C_{50}H_{102}$), which are described as $[R+CpCo\text{-}2H_2]^+$ cations, where R corresponds to an *n*-alkane. In one study, a methodology was successfully employed for high-molecular-weight *n*-paraffin analysis by MALDI time-of-flight mass spectrometry [9]. Lorente et al. [9] proposed the use of urea solutions and $AgNO_3$ on thin layer chromatography (TLC) plates. However, the mass spectra showed high intensity for interferent signals in the *m/z* region < 400. These signals were considered to emerge from the interactions between the silica of the TLC plates and the $AgNO_3$ matrix.

Ionization studies using different ion source gases, such as nitrogen (N_2), oxygen (O_2), helium (He), synthetic air, and carbon dioxide (CO_2), were used in the ionization of saturated and unsaturated HCs by mass spectrometry and hyphenated techniques [23–26]. Although polar and nonpolar compounds can be easily ionized by the APCI source, one of its greatest applications in petroleomics is in paraffin analysis [14,15,23,27]. APCI source was developed in 1970 [28], and it is based on corona discharge ionization followed by ion–molecule reactions at atmospheric pressure [23]. Generally, ions can be formed in three different ways: (1) as radical cation–ionization by Penning ($[M]^{\cdot+}$) [29], (2) by proton transfer [29], hydride abstraction [24] ($[M+H]^+$, or $[M-H]^+$); or (3) from the formation of adducts [29] ($[M+CH_4]^+$, $[M+NH_4]^+$, *etc.*). In the APCI source, gases have the function of nebulizing the liquid sample, thus promoting the ionic desolvation [29]. When ionized by the corona discharge, nebulizer gases can act as a reagent gas and a primary ions source, desolvating and transferring charge to the analyte simultaneoulsy [23,29].

Nyadong et al. [25] analyzed saturated HC mixture by atmospheric pressure laser-induced acoustic desorption chemical ionization (AP/LIAD-CI) using O_2 as the carrier/reagent gas. Jin et al. [23] studied field ionization mass spectrometry with APCI-MS to determine the distribution of HCs in commercial standards and in lubricating oils. They used O_2 and N_2 as ion source gases to examine the ionization of samples and concluded that the APCI/O_2/hexane system produced $[M-H]^+$ ions predominantly.

Atmospheric pressure ionization (API) mass spectrometry was applied to polyaromatic hydrocarbon (PAH) standards [30,31]. Ghislain et al. [31] used a complex mixture of PAHs and oxy-PAHs to compare the ionization of different ionization sources, such as ESI, APPI, and APCI, using a Q-TOF mass spectrometer. The authors observed the formation of $M^{\cdot+}$ and $[M+H]^+$ ions for PAH and oxy-PAH compounds from the APCI(+) source. They also evaluated the influence of different solvents on the ionization of these compounds, concluding that *n*-hexane provided the best ionization for high molecular weight PAH compounds [31].

The mechanism that best explains the ionization of linear HCs is hydride abstraction, which is the formation of $[M-H]^+$ ions. Tose et al. [14] observed that linear, cyclic, and branched paraffins have their ionization favored by the use of HCs with carbon numbers (CN) between C_5 and C_8 as reagents in the APCI source. Among them, the isooctane provided the best results when used as a solvent/reagent. Scheme 1 describes the steps for the ionization mechanism proposed for the HCs [14,24]. In step **I**, the ion source gas is ionized with the formation of primary ions [ionization energy: O_2 (12.1 eV) [25]; N_2 (15.6 eV) [25], and He (24.6 eV) [24]. In step **II**, the primary ion (ion source gas$^{1\cdot+}$) transfers its excess energy to the solvent, forming the radical cation $[C_8H_{18}{}^{\cdot+}]*$. In step **III**, the radical cation is highly reactive and produces two fragments, a tertiary radical and a $C_4H_9^+$ cation. In step **IV**, the $C_4H_9^+$ cation reacts with the isooctane molecule to abstract a hydride and finally form the reactant ion ($[C_8H_{18}\text{-}H]^+$). In step **V**, the $[C_8H_{18}\text{-}H]^+$ cation ionizes the analyte to form the $[M-H]^+$ species.

In the present study, an ionization mechanism similar to Scheme 1 is suggested to form the $[M+H]^+$ ions observed from condensed aromatic (CA) compounds by using APCI(+). Scheme 2 shows the proposed steps for the ionization mechanism of CA compounds. **Steps I**, **II**, and **III** are similar to the previously proposed ionization scheme for the aliphatic,

I) Ion source gas + e^- → Ion source gas$^{1\cdot+}$ + 2e^-

II) Ion source gas$^{1\cdot+}$ + C_8H_{18} → $([C_8H_{18}]^{\cdot+})^*$ + Ion source gas

III) $([C_8H_{18}]^{\cdot+})^*$ → $C_4H_9^{\cdot}$ + $C_4H_9^+$

IV) $C_4H_9^+$ + C_8H_{18} → $[C_8H_{18}\text{-}H]^+$ + C_4H_{10}

V) $[C_8H_{18}\text{-}H]^+$ + M → $[M\text{-}H]^+$ + C_8H_{18}

Scheme 1. The proposed ionization mechanism by the APCI(+) source for saturated HCs using isooctane as a solvent/reagent. Adapted scheme from the literature [14,24].

I) Ion source gas + $e^- \rightarrow$ Ion source gas$^{+\cdot}$ + 2e^-

II) Ion source gas$^{+\cdot}$ + $C_8H_{18} \rightarrow ([C_8H_{18}]^{+\cdot})^*$ + Ion source gas

III) $([C_8H_{18}]^{+\cdot})^* \rightarrow C_4H_9^{\cdot} + C_4H_9^+$

IV) $C_4H_9^+ + M \rightarrow [M+H]^+ + C_4H_8$

Scheme 2. The proposed ionization mechanism by the APCI(+) source for the ionization of CAs using isooctane as a solvent/reagent.

cyclic, and branched HCs. In **step IV**, a different mechanism is proposed: the $C_4H_9^+$ radical ionizes the analyte through proton transfer to form the $[M+H]^+$ species instead of reacting with the isooctane as previously proposed in Scheme 1. According to Owen et al. [32] carbon disulfide (CS_2) can also be used to ionize HCs and CAs but only through Penning ionization, $M^{\cdot +}$ because it does not contain hydrogen atoms to promote the ionization for proton transfer or hydride abstraction [32].

This study aimed to compare the ionization efficiency of HC and CA standards as well as paraffin fractions using three different ion source gases (synthetic air, N_2 and He) combined with the APCI(+)FT-ICR mass spectrometer. Among the samples are three HC and CA standards, a paraffin reference standard used for gas chromatography with flame ionization (GC-FID) calibration (C_5-C_{120}), and two saturated HC fractions produced from Brazilian petroleum samples.

2. Experimental

2.1. Reagents and samples

Three different types of model HC compounds were used: cyclic (5-α-cholestane, ≥97%, HPLC), branched (squalene, ≥98%), and linear (hexatriacontane, 98%) HC standards. Three CA standards [coronene (≥99%, HPLC), benz[a]anthracene (98%, HPLC), and N,N′-bis(3-pentyl)perylene-3,4,9,10-bis(dicarboximide) (≥99%, HPLC)] were also studied. All standards were supplied by Sigma–Aldrich Chemicals (USA). One *n*-paraffin standard, which contained CN ranging from C_5 to C_{120}, was supplied by AC 655 (USA), with analytical grade purity higher than 99.5%. It is typically used as a reference material for GC-FID calibration. Two saturated HC fractions were examined: one obtained from the fractionation of crude oil using the saturated, aromatic, and polar (SAP) method (fraction SA_1) and the other by a commercial petrochemical process (fraction SA_2) (CENPES/Petrobras, Brazil).

The SAP method was performed in an open chromatography column, where approximately 4 g of silica (70–230 mesh) was activated at 120 °C for 12 h. The silica was packed into a glass column of 12 cm. Crude oil of 50 mg was added to the top of the column. Successive elution was performed with 35 mL of hexane (99% PA), 50 mL of dichloromethane:hexane 9:1 (% v/v) (99% PA), and 40 mL of methanol (99.9%, HPLC) to separate the fractions of saturates, aromatic, and polar compounds, respectively. The fraction SA_1 was allowed to dry at ambient temperature. The percentage of this saturated fraction was 58.2 ± 3.9 wt%.

Acetonitrile and sodium trifluoroacetate (NaTFA) with analytical grade purity > 99.99% were purchased from Sigma–Aldrich and used for the FT-ICR MS calibration. Isooctane was supplied by Vetec Química Fina Ltda. (Brazil), and it was used in the paraffin solution preparation and as an APCI reagent. All reagents were used as received without any further purification. Synthetic air (20% of O_2; 80% of N_2-grade FID 99.999%) as well as N_2 and He, which were both of analytical grade (5.0 and 99.999%), were purchased from White Martins/Praxair Inc. (Brazil) and tested as the ion source gas at the APCI source.

2.2. APCI(+)-MS

FT-ICR MS analysis was performed using a 9.4 T Q-FT-ICR MS hybrid (Solarix, Bruker Daltonics, Bremen, Germany) equipped with a commercial APCI (Bruker Daltonics, Bremen, Germany) source set to operate over *m/z* 200–2000. All samples were analyzed using the positive ionization mode APCI(+).

The CA samples were diluted in isooctane:CS_2 solutions (2:1), and the HC standards and paraffins samples (fractions) were diluted in isooctane at a concentration of 0.5 mg mL^{-1}. The resultant solution was sonicated for 15 min at 40 °C and directly infused at a flow rate of 20–40 μL min^{-1}. The efficiency of HC ionization in the paraffin samples was evaluated as a function of the type of ion source gas used (synthetic

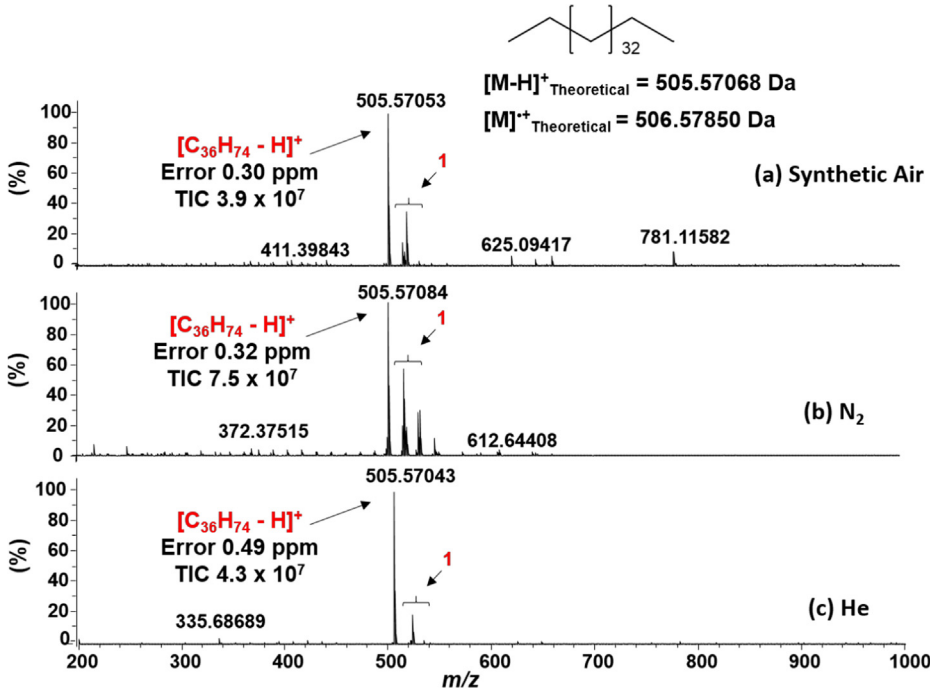

Fig. 1. APCI(+)FT-ICR mass spectra of hexatriacontane using different types of ion source gases: (a) synthetic air, (b) N_2, and (c) He. Number 1 (highlighted in red) indicates the *m/z* 520–560 region, where oxygenated and nitrogenous species can be found. The assigned molecular formulas of this standard are summarized in Table 1. (For interpretation of the references to colour in this figure legend, the reader is referred to the web version of this article.)

Table 1
Assigned molecular formula, mass accuracy (in ppm), and measured and theoretical *m/z* obtained from APCI(+)FT-ICR MS data for the hexatriacontane molecule as a function of ion source gases (synthetic air, N_2, and He).

	Gas	Measured *m/z*	Theoretical *m/z*	Error (ppm)	Ions	TIC	TIC (%)
Hexatriacontane	Synthetic	235.16943	235.16926	0.72	$[C_{15}H_{23}+O_2]^{rad+}$	6.4×10^5	1.6
Hexatriacontane	Air	258.24285	258.24276	0.35	$[C_{15}H_{32}+NO_2]^{rad+}$	6.6×10^5	1.7
		272.25860	272.25841	0.70	$[C_{16}H_{34}+NO_2]^{rad+}$	8.4×10^5	2.2
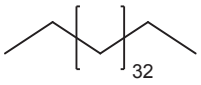		286.27416	286.27406	0.35	$[C_{17}H_{36}+NO_2]^{rad+}$	7.4×10^5	1.9
		309.35169	309.35158	0.36	$[C_{22}H_{45}]^{rad+}$	8.0×10^5	2.0
		323.36730	323.36723	0.22	$[C_{23}H_{47}]^{rad+}$	7.4×10^5	1.9
		337.38295	337.38288	0.21	$[C_{24}H_{49}]^{rad+}$	9.4×10^5	2.4
		371.31556	371.31559	0.08	$[C_{22}H_{43}+O_4]^{rad+}$	1.4×10^6	3.7
		393.44551	393.44548	0.08	$[C_{28}H_{57}]^{rad+}$	1.0×10^6	2.7
		411.39843	411.39853	0.24	$[C_{30}H_{51}]^{rad+}$	1.6×10^6	4.1
		435.49232	435.49243	0.25	$[C_{31}H_{63}]^{rad+}$	1.1×10^6	2.8
		503.55476	503.55503	0.54	$[C_{36}H_{71}]^{rad+}$	9.0×10^5	2.3
		505.57053	505.57068	0.30	$[C_{36}H_{74}\text{-}H]^+$	3.9×10^7	100
		506.57381	506.57405	0.47	$[^{13}C^{12}C_{35}H_{74}\text{-}H]^+$	1.6×10^7	40.0
		507.57725	507.57740	0.30	$[^{13}C_2{}^{12}C_{34}H_{74}\text{-}H]^+$	3.3×10^6	8.5
		519.54975	519.54994	0.37	$[C_{36}H_{71}+O]^{rad+}$	6.1×10^6	15.8
		521.56541	521.56559	0.35	$[(C_{36}H_{74}\text{-}H)+O]^+$	3.7×10^6	9.5
		523.58105	523.58124	0.36	$[(C_{36}H_{74}\text{-}H)+O]^+$	1.4×10^7	36.0
		535.54475	535.54486	0.21	$[C_{36}H_{71}+O_2]^{rad+}$	1.3×10^6	3.4
		547.58098	547.58124	0.47	$[C_{38}H_{75}+O]^{rad+}$	8.1×10^5	2.1
		561.63291	561.63328	0.66	$[C_{40}H_{81}]^{rad+}$	8.8×10^6	2.3
		1026.12854	1026.12900	0.45	$[C_{72}H_{145}+O]^{rad+}$	3.6×10^6	9.2
	N_2	220.20621	220.20598	1.04	$[C_{15}H_{26}+N]^{rad+}$	5.4×10^6	7.3
		234.22124	234.22163	1.67	$[C_{16}H_{28}+N]^{rad+}$	8.0×10^5	1.1
		252.19601	252.19581	0.79	$[C_{15}H_{26}+NO_2]^{rad+}$	4.7×10^6	6.2
		258.24293	258.24276	0.66	$[C_{15}H_{32}+NO_2]^{rad+}$	8.7×10^5	1.2
		272.25860	272.25841	0.70	$[C_{16}H_{34}+NO_2]^{rad+}$	1.3×10^6	1.8
		286.27421	286.27406	0.52	$[C_{17}H_{36}+NO_2]^{rad+}$	9.9×10^5	1.3
		288.28988	288.28971	0.59	$[C_{17}H_{38}+NO_2]^{rad+}$	1.9×10^6	2.6
		309.35171	309.35158	0.42	$[C_{22}H_{45}]^{rad+}$	1.6×10^6	2.2
		323.36741	323.36723	0.56	$[C_{23}H_{47}]^{rad+}$	1.5×10^6	2.0
		337.38304	337.38288	0.47	$[C_{24}H_{49}]^{rad+}$	2.0×10^6	2.7
		371.36730	371.36723	0.19	$[C_{27}H_{47}]^{rad+}$	1.7×10^6	2.2
		393.44552	393.44548	0.10	$[C_{28}H_{57}]^{rad+}$	2.9×10^6	3.8
		407.46125	407.46113	0.29	$[C_{29}H_{59}]^{rad+}$	2.9×10^6	3.9
		421.47684	421.47678	0.14	$[C_{30}H_{61}]^{rad+}$	2.8×10^6	3.8
		435.49243	435.49243	0.00	$[C_{31}H_{63}]^{rad+}$	2.2×10^6	2.9
		450.50339	450.50333	0.13	$[C_{31}H_{64}+N]^{rad+}$	2.1×10^6	2.8
		464.51905	464.51898	0.15	$[C_{32}H_{66}+N]^{rad+}$	1.6×10^6	2.2
		478.53466	478.53463	0.06	$[C_{33}H_{68}+N]^{rad+}$	2.1×10^6	2.8
		492.55030	492.55028	0.04	$[C_{34}H_{70}+N]^{rad+}$	2.6×10^6	3.4
		503.55503	503.55503	0.00	$[C_{36}H_{71}]^{rad+}$	3.7×10^6	5.0
		504.56291	–	–	–	9.2×10^6	12.2
		505.57084	505.57068	0.32	$[C_{36}H_{74}\text{-}H]^+$	7.5×10^7	100
		506.57413	506.57405	0.16	$[^{13}C^{12}C_{35}H_{74}\text{-}H]^+$	3.4×10^7	45.8
		507.57746	507.57740	0.12	$[^{13}C_2{}^{12}C_{34}H_{74}\text{-}H]^+$	6.9×10^6	9.3
		519.54999	519.54994	0.10	$[C_{36}H_{71}+O]^{rad+}$	1.5×10^7	19.7
		521.56573	521.56559	0.27	$[C_{36}H_{73}+O]^{rad+}$	2.8×10^7	37.6
		523.58132	523.58124	0.15	$[C_{36}H_{75}+O]^{rad+}$	1.4×10^7	19.2
		534.59726	534.59723	0.06	$[C_{37}H_{73}+N]^{rad+}$	2.2×10^7	28.7
		536.57653	536.57649	0.07	$[C_{36}H_{74}+NO]^{rad+}$	2.2×10^7	29.7
		550.59224	550.59214	0.18	$[C_{37}H_{76}+NO]^{rad+}$	8.8×10^6	11.7
		576.64424	576.64418	0.10	$[C_{40}H_{82}+N]^{rad+}$	2.2×10^6	3.0
		610.62858	610.62853	0.08	$[C_{43}H_{80}+N]^{rad+}$	2.1×10^6	2.8
		612.64408	612.64418	0.16	$[C_{43}H_{82}+N]^{rad+}$	3.2×10^6	4.4
		1026.12960	1026.12900	0.58	$[C_{72}H_{145}+O]^{rad+}$	1.8×10^6	2.4
	He	261.09144	261.09101	1.65	$[C_{18}H_{13}+O_2]^{rad+}$	5.9×10^5	1.4
		303.20186	–	–	–	5.6×10^5	1.3
		335.68689	–	–	–	1.7×10^6	4.0
		365.41404	365.41418	0.38	$[C_{26}H_{53}]^{rad+}$	7.1×10^5	1.7
		379.42977	379.42983	0.16	$[C_{27}H_{55}]^{rad+}$	6.7×10^5	1.6
		393.44529	393.44548	0.48	$[C_{28}H_{57}]^{rad+}$	9.8×10^5	2.3
		407.46081	407.46113	0.79	$[C_{29}H_{59}]^{rad+}$	9.1×10^5	2.1
		421.47663	421.47678	0.36	$[C_{30}H_{61}]^{rad+}$	1.0×10^6	2.4
		435.49223	435.49243	0.46	$[C_{31}H_{63}]^{rad+}$	7.9×10^5	1.9
		449.50774	449.50808	0.76	$[C_{32}H_{65}]^{rad+}$	5.1×10^5	1.2
		463.52347	463.52373	0.56	$[C_{33}H_{67}]^{rad+}$	3.9×10^5	0.9
		504.56275				6.2×10^5	1.5
		505.57043	505.57068	0.49	$[C_{36}H_{74}\text{-}H]^+$	4.3×10^7	100
		506.57383	506.57405	0.43	$[^{13}C^{12}C_{35}H_{74}\text{-}H]^+$	1.5×10^7	35.6
		507.57717	507.57740	0.45	$[^{13}C_2{}^{12}C_{34}H_{74}\text{-}H]^+$	2.8×10^6	6.6
		519.54944	519.54994	0.96	$[C_{36}H_{71}+O]^{rad+}$	5.9×10^5	1.4

(*continued on next page*)

Table 1 (*continued*)

Gas	Measured *m/z*	Theoretical *m/z*	Error (ppm)	Ions	TIC	TIC (%)
	521.56536	521.56559	0.44	$[C_{36}H_{73}+O]^{rad+}$	1.1×10^6	2.6
	522.59699	522.59723	0.46	$[C_{36}H_{76}+N]^{rad+}$	1.1×10^6	2.6
	523.58102	523.58124	0.42	$[C_{36}H_{75}+O]^{rad+}$	8.3×10^6	19.6
	534.59705	534.59723	0.34	$[C_{37}H_{76}+N]^{rad+}$	1.2×10^6	2.8
	1026.12697	1026.12900	1.98	$[C_{72}H_{145}+O]^{rad+}$	7.5×10^5	1.8

air, N_2, and He). The APCI(+) source conditions were as follows: ion source gas temperature and pressure of 320 °C and 2.0 bar, respectively, capillary voltage of 2.5–3.1 kV, transfer capillary temperature of 180 °C, drying gas of 1–4 L min^{-1}, end plate offset of 500 V, skimmer of 30–40 V, collision voltage of − 5 V and 12 V, and a corona discharge of 3000–9000nA. The parameters for each type of ion source gas employed are summarized in the Supplementary material (Table 1S). Analyzes of paraffin fractions were performed in duplicate.

In the FT-ICR MS analyzer, a 0.02 s ion accumulation time was used in the hexapole followed by sample transport to the analyzer cell (ICR) through the multipole ion guide system (another hexapole). Each spectrum was acquired using 200 scans of time-domain transient signals in 4 megapoint time-domain data sets. The front and back trapping voltages in the ICR cell were +0.80 V and +0.85 V, respectively, for positive ionization mode. All mass spectra were externally calibrated using L-arginine (200–2000 *m/z*), then internally recalibrated using the most abundant homologous alkylated compounds in each sample. The resolving power ($m/\Delta m_{50\%}$ from 450,000 to 550,000 at *m/z* 400, where $\Delta m_{50\%}$ is the full width at half-maximum peak height) and < 1 ppm mass accuracy provided the unambiguous molecular formula assignments for all singly charged molecular ions. The APCI(+) mass spectra were acquired and processed with a custom algorithm specifically developed for the petroleum data Composer software (Sierra Analytics, Pasadena, CA, USA). The MS data were processed, and the elemental composition of the sample was determined by measuring the *m/z* values. Compound class diagrams, DBE distributions, and DBE versus CN were plotted to help interpret the results. The unsaturation level of each compound could be deducted directly from its DBE value.

3. Results and discussion

3.1. Hydrocarbon standards

Fig. 1a–c show the APCI(+)FT-ICR mass spectra of hexatriacontane using three different types of ion source gases: synthetic air (Fig. 1a), N_2 (Fig. 1b), and He (Fig. 1c). Note that the hexatriacontane was detected only through hydride abstraction ($[M-H]^+$, *m/z* 505, Fig. 1) in all cases, thus proving that this ionization mechanism preferentially occurred in the presence of linear HC compounds. The region of *m/z* 520–560 (identified by number 1 in Fig. 1a–c) indicates the existence of oxygenated and nitrogenous species, which are preferentially formed when synthetic air and N_2 are used as ion source gases (Fig. 1a, b). In analyzing the ionic species formed in the 5-α-cholestane and squalene standards, two [electron transfer ($[M]^{+\cdot}$) and hydride abstraction ($[M-H]^+$), Fig. 1S and 3S] and three ($[M^{+\cdot}]$, $[M-H]^+$, and $[M+M+H]^+$, Fig. 2S and 4S) ionization mechanisms were observed, respectively. Moreover, nitrogenated and oxygenated HC species (with a relative abundance of up to 38%) and fragmentation products were also produced. All the assigned molecular formula, DBE, and mass accuracy for the hexatriacontane, 5-α-cholestane, and squalene compounds are summarized in Tables 1, S2, and S3, respectively.

In comparing the effects of ion source gas on 5-α-cholestane, the use of synthetic air preferentially formed $[M-H]^+$ ions, with *m/z* 371.36719 and total ionic current (TIC) in the order of 10^8 (Fig. 1Sa). N_2 (Fig. 1Sb) and He (Fig. 1Sc) gases showed higher abundance of $[M^{+\cdot}]$ ions, with *m/z* 372.37503 and 372.37504 and TIC of 10^8 and 10^7, respectively. Squalene ions were mostly obtained by proton transfer on the three gases used, with $[M+H]^+$ ions of *m/z* 411.39860 for synthetic air, *m/z* 411.39879 for N_2, and *m/z* 411.39841 for He (Fig. 2S). The $[M-H]^-$ species, which was detected through hydride abstraction, had an relative abundance < 12%. However, for the squalene, $[C_{31}H_{54}+N]^{\cdot+}$ ion, higher relative abundance values were observed with the use of N_2 and He gases, being close to 58 and 25%, respectively.

An expanded insert of Fig. 1 is shown in Fig. 2, and it features the region of *m/z* 504–509 of the APCI(+) mass spectra referring to the hexatriacontane analysis. The isotopologue profile of the hexatriacontane is resolved for the ions of *m/z* 505–507 ($M_1 = [^{12}C_{36}H_{74}\text{-}H]^+$, *m/z* 505; $M+1 = [^{13}C_1{}^{12}C_{35}H_{74}\text{-}H]^+$, *m/z* 506, and $M+2 = [^{13}C_2{}^{12}C_{34}H_{74}\text{-}H]^+$, *m/z* 507).

Fig. 3Sa–c presents an expansion in the *m/z* 369–375 region of the APCI(+) mass spectra, as shown in Fig. 1Sa–c, and it refers to the isotopologue profile of 5-α-cholestane. The insert highlights the importance of using ultra-high resolution instruments in petroleomics. FT-ICR MS can resolve the isotopologue profile of 5-α-cholestane between the two ionic species detected: $M^{\cdot+}$ radical-ion ($M = [^{12}C_{27}H_{48}]^{\cdot+}$, *m/z* 372; $M+1 = [^{13}C_1{}^{12}C_{26}H_{48}]^{\cdot+}$, *m/z* 373 and $M+2 = [^{13}C_2{}^{12}C_{25}H_{48}]^{\cdot+}$, *m/z* 374) and hydride abstraction ($M_1 = [^{12}C_{27}H_{48}\text{-}H]^+$, *m/z* 371; $M_1+1 = [^{13}C_1{}^{12}C_{26}H_{48}\text{-}H]^+$, *m/z* 372, $M_1+2 = [^{13}C_2{}^{12}C_{25}H_{48}\text{-}H]^+$, *m/z* 373 and $M_1+3 = [^{13}C_3{}^{12}C_{24}H_{48}\text{-}H]^+$, *m/z* 374). The ions and their isotopes in the *m/z* 371–374 region were resolved with a resolution power in the order of 400,000. In all cases, the signals were detected with a mass accuracy lower than 2 ppm. A similar behavior was observed for the squalene (Fig. 4S). The theoretical values were obtained by the Data Analysis *software*, (Bruker Daltonics), and the assignment of the molecules are summarized in Table 6S.

As shown in the APCI(+)FT-ICR MS data in Figs. 2, 3S, and 4S, synthetic air and He gases presented better mass accuracy in the detection of HC standards, except for hexatriacontane. The mass accuracy range found for the HC standards is shown in Table 2: 0–0.49 ppm for He, 0.02–0.68 ppm for synthetic air, and 0.03–2.03 ppm for N_2.

Fig. 3 shows a histogram containing the relative abundance of the signals attributed to the isotopologue profile of **(3a)** hexatriacontane, **(3b)** 5-α-cholestane, and **(3c)** squalene as a function of the ion source gas employed. This histogram visualizes the relative abundance of the assigned molecular formula to each HC standard. Comparing the effects of the ion source gas on the relative abundance values of the detected species, He favored the formation of the $[M]^{\cdot+}$ and $[M-H]^+$ ions for 5-α-cholestane **(3b)**, and synthetic air mostly produced ions through the abstraction of hydrides. For squalene **(3c)**, despite all gases favoring the ionization through transfer proton, He also presents a better

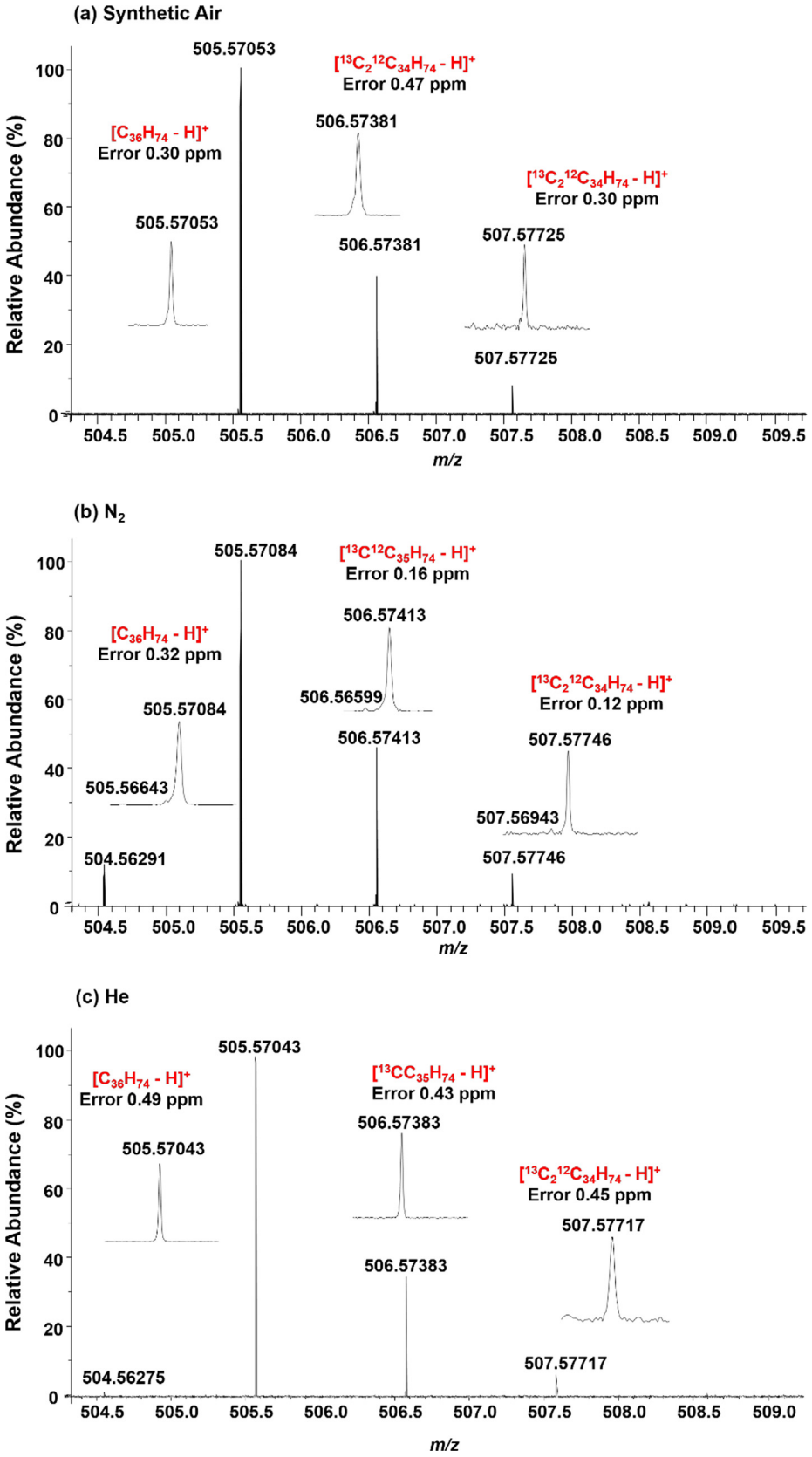

Fig. 2. Expanded insert in the *m/z* 504–509 region of the APCI(+) mass spectra (Fig. 1) for hexatriacontane using three ion source gases: synthetic air (a), N_2, (b), and He (c).

Table 2
Mass accuracy (in ppm) of the HC and CA standards as a function of different ion source gases.

Standards	Ion source Gas Error (ppm)		
	Synthetic Air	N_2	He
Hexatriacontane	0.30–0.47	0.12–0.32	0.43–0.49
5-α-Cholestane	0.02–0.21	0.03–0.37	0.00–0.16
Squalene	0.17–0.68	0.63–1.06	0.05–0.29
Coronene	0.10–0.33	1.89–2.03	0.03–0.43
Benz[a]anthracene	0.17–0.39	0.65–0.74	0.17–0.35
N,N′-bis(3-pentyl)perylene-3,4,9,10-bis (dicarboximide)	0.13–0.34	0.94–1.37	0.13–0.43

performance in the formation of ions through the abstraction of hydrides.

3.2. CA standards

Fig. 4a–c shows the APCI(+)FT-ICR mass spectra for the coronene molecule acquired with three different types of ion source gases: synthetic air (Fig. 4a), N_2 (Fig. 4b), and He (Fig. 4c). Identifying the existence of two ionization mechanisms, namely, electron transfer ($[M]^{+\cdot}$) and proton transfer ($[M+H]^+$) (scheme 2), was possible in all cases. In addition to the production of $[M^{+\cdot}]$ and $[M+H]^+$ species, the formation of nitrogenous and oxygenated species (relative abundance < 5%) as well as fragmentation products also occurred Table 3. Similar results were obtained by the other CA standards [benz[a]anthracene and N,N′-bis(3-pentyl)perylene-3,4,9,10-bis(dicarboximide)], as shown in Figs. 5S and 6S, respectively.

Comparing the effects of the ion source gas on the coronene, for synthetic air and N_2, coronene was mostly detected as a molecular ion, $[M]^{+\cdot}$, with *m/z* 300.0934 and *m/z* 300.0939 and TIC in the order of 10^8 and 10^7, respectively (Fig. 4a, b). Signals with *m/z* < 300 and the presence of contaminants containing values of *m/z* 391, 625, and 78, which appear randomly independent of the type ion source gas employed, were observed in both cases. Oxygenated and nitrogenous species were also detected (*m/z* 314–317, Table 3). In contrast to the results observed with the use of synthetic air and N_2, He provides a cleaner APCI(+) mass spectrum, that is, with minimal fragmentation or analyte oxidation. Coronene was identified mainly through proton transfer, $[M+H]^+$, *m/z* 301.1011, with a mass accuracy of 0.13 ppm and TIC in the order of 10^8 (Fig. 4c). A similar behavior was observed for the other two CA standards studied, benz[a]anthracene and N,N'-bis (3-pentyl)perylene-3,4,9,10-bis(dicarboximide), as shown in Figs. 5S and 6S, respectively. He generated APCI(+) mass spectra containing a low intensity of interferent signals (*m/z* 285, 290, 505, 625, 661, and 781, Figs. 5S and 6S) and exhibited minimal fragmentation (*m/z* 265, Fig. 6Sb) compared to the N_2. For both analytes, synthetic air showed ionization efficiency (signal-to-noise ratio) analogous to He; that is, no impurity signals were detected for benz[a]anthracene (Fig. 5S). Furthermore, in all cases, benz[a]anthracene (Fig. 5S) was mainly identified as a molecular ion ($M^{+\cdot}$, $M = C_{18}H_{12}$, *m/z* 228.0935, and error ≤ 0.66 ppm), and N,N'-bis(3-pentyl)perylene-3,4,9,10-bis(dicarboximide) (Fig. 6S) was observed as a protonated molecule ($[M+H]^+$, where $M = C_{34}H_{30}N_2O_4$, *m/z* 531.2283, error < 1 ppm). Finally, nitrogenous and oxygenated species were also observed with an relative abundance < 5% (*m/z* 242–245, Table 4S, and *m/z* 544–547, Table 5S).

Fig. 5a–c show an expansion of the *m/z* 300–303 region of the APCI (+) mass spectra presented in Fig. 4a–c, which refers to the isotopologue profile of coronene. FT-ICR MS can resolve the isotopologue profile of coronene between the two detected ionic species, namely, $[M]^{\cdot+}$ radical-ion ($M = [^{12}C_{24}H_{12}]^{\cdot+}$, *m/z* 300; $M+1 = [^{13}C_1{}^{12}C_{23}H_{12}]^{\cdot+}$, *m/z* 301; and $M+2 = [^{13}C_2{}^{12}C_{22}H_{12}]^{\cdot+}$, *m/z* 302 species) and protonated cation ($M_1 = [^{12}C_{24}H_{12}+H]^+$, *m/z* 301; and $M_1+1 = [^{13}C_1{}^{12}C_{23}H_{12}+H]^+$, *m/z* 302, species). The ions of *m/z* 301 and 302 ($[^{13}C_1{}^{12}C_{23}H_{12}]^+$ and $[^{12}C_{24}H_{12}+H]^+$) as well as their isotopes ($[^{13}C_2{}^{12}C_{22}H_{12}]^{\cdot+}$ and $[^{13}C_1{}^{12}C_{23}H_{12}+H]^+$) were resolved by their mass defect difference of 4.4 mDa and a resolution power in the order of 400,000. In all cases, the signals were detected with a mass

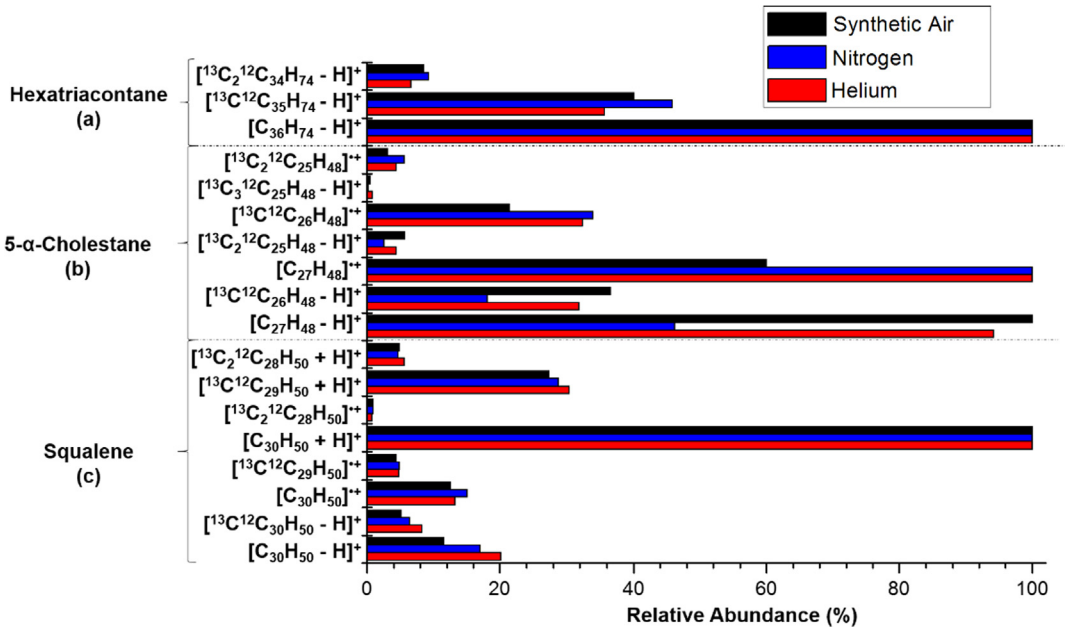

Fig. 3. Relative abundance of the isotopologue profile (M, M+1, M+2, and M+3) of the ($[M]^{\cdot+}$), $[M-H]^+$, and $[M+H]^+$ species of HC standards in the function of different types of ion source gases: (a) hexatriacontane, (b) 5-α-cholestane, and (c) squalene.

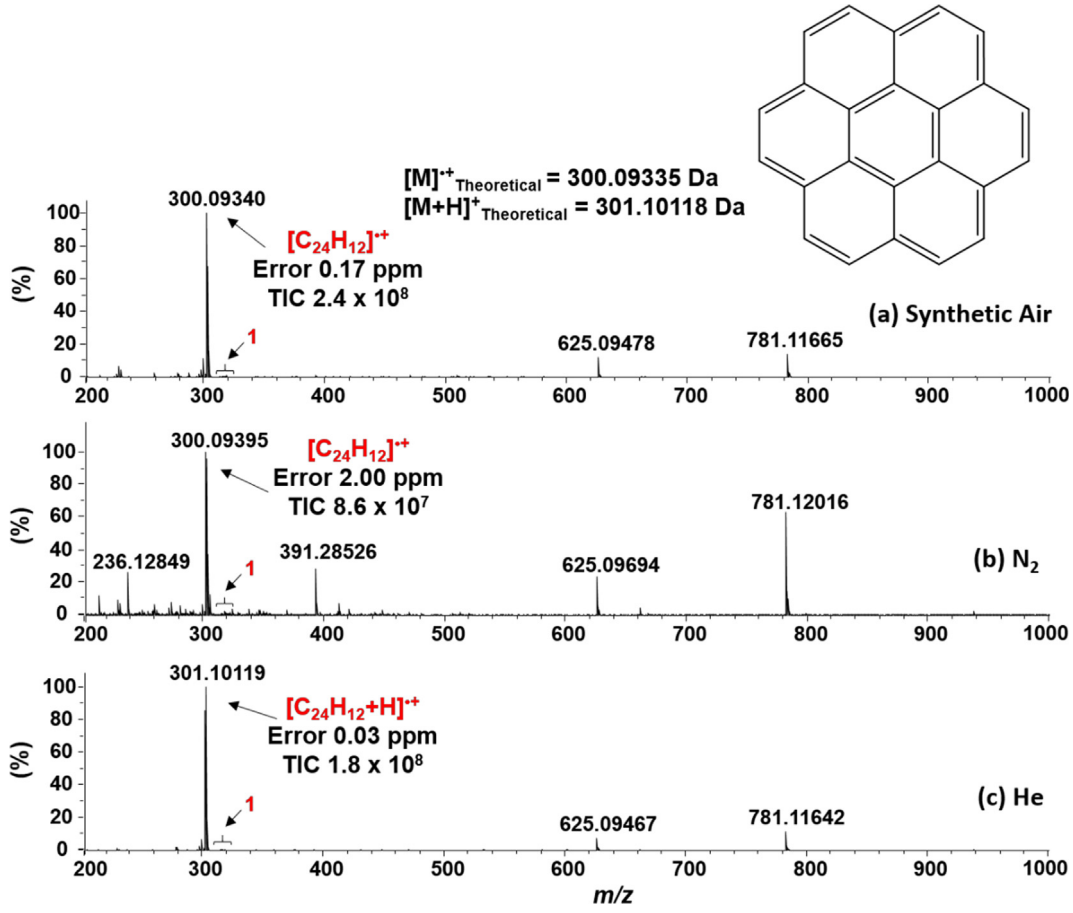

Fig. 4. APCI(+)FT-ICR mass spectra of coronene using different types of ion source gases: (a) synthetic air, (b) N_2, (c) He. Number (1) indicates the *m/z* region where oxygenated and nitrogenous species can be found. Their molecular formulas are summarized in Table 3.

accuracy lower than 2 ppm.

An expanded insert of Fig. 5S is illustrated in Fig. 7S, which shows the *m/z* 228–230 region of the APCI(+) mass spectra referring to the analysis of benz[a]anthracene. The isotopologue profile of benz[a]anthracene was resolved for the ions of *m/z* 229 ($M+1 = [^{13}C_1{}^{12}C_{17}H_{12}]^{\cdot+}$ and $M_1 = [^{12}C_{18}H_{12}+H]^+$ species) and *m/z* 230 ($M+2 = [^{13}C_2{}^{12}C_{16}H_{12}]^{\cdot+}$ and $M_1+1 = [^{12}C_{17}{}^{13}C_1H_{12}+H]^+$ species), with a mass defect difference of 4.4 mDa. A similar behavior was observed for the N,N′-bis(3-pentyl)perylene-3,4,9,10-bis(dicarboximide), as shown in Fig. 8S.

According to the results in Figs. 5 and 7S-8S, synthetic air and He ion presented better mass accuracy in the detection of all three CA standards studied. The mass accuracy range for coronene, benz[a]anthracene, and N,N′-bis(3-pentyl)perylene-3,4,9,10-bis(dicarboximide) and their isotopologues profile are presented in Table 2.

The histogram (Fig. 6) shows the relative abundance of the assigned signals to the corresponding ions in the mass spectra (Figs. 5, 7S, and 8S) as well as the signals of the isotopologue profile of the CA standards detected as a function of the ion source gases employed. One reasonable explanation for how the reagent ion promotes the ionization of the analyte can be found in the gas phase basicity (GB) or proton affinity data. GB was previously calculated for coronene and benzanthracene (836.8 and 841.0 kJ mol^{-1}) [33]. The N,N′-bis(3-pentyl)perylene-3,4,9,10-bis(dicarboximide) standard does not have the GB values described in the literature, but it has a structure similar to perylene, which has a GB of 859.4 kJ mol^{-1} [32]. This value is higher than those obtained for other compounds. In addition, N,N′-bis(3-pentyl)perylene-3,4,9,10-bis(dicarboximide) has a protonatable heteroatom structure, which makes it even more susceptible to protonated molecule formation, $[M+H]^+$. This result was experimentally confirmed, as n,n′-bis(3-pentyl)perylene-3,4,9,10-bis(dicarboximide) showed a greater abundance of protonated species regardless of the type of gas used. Comparing the effects of the ion source gas on the relative abundance values of the detected species for coronene and benzanthracene, He favored the ionization by the proton transfer mechanism, $[M+H]^+$ species, in which the relative abundance was considerably high for the following species: $[^{12}C_{24}H_{12}+H]^+$, $[^{12}C_{18}H_{12}+H]^+$, and $[^{13}C_1{}^{12}C_{17}H_{12}+H]^+$ (Fig. 6a, b). Conversely, the N_2 and synthetic air ion source gases favored the detection of the CAs by both ionization mechanisms of Penning ($M^{\cdot+}$) and protonation ($[M+H]^+$).

3.3. Formation of nitrogenated or oxygenated species

Synthetic air is a mixture of O_2 and N_2 (20:80 v/v%). Because its higher N_2 content, it is expected to have an ionization performance similar to that of N_2. Surprisingly, synthetic air showed a performance superior to that of N_2, with better mass accuracy, lower matrix suppression, and higher signal-to-noise ratio than N_2 gas. This better performance can be attributed to the ionizing capacity of O_2 on the HC and CA molecules. Nyadong et al. [25] studied the ionization of saturated HC mixtures using O_2 as the carrier/reagent gas by the AP/LIAD-CI source. A higher sensitivity was observed for O_2 in the order of 2.5-fold

Table 3
Assigned HC species in the *m/z* 300–303 region of the APCI(+)-MS of the coronene molecule as a function of ionizing gas: synthetic air, N_2, and He.

	Gas	Measured *m/z*	Theoretical *m/z*	Error (ppm)	Ions	TIC	TIC (%)
Coronene 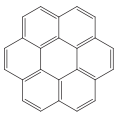	Synthetic Air	211.97836	–	–	–	–	1.18
		228.09343	–	–	–	–	6.51
		236.12820	–	–	–	–	0.98
		257.24762	–	–	–	–	3.00
		276.09347	–	–	–	–	2.89
		277.10130	–	–	–	–	1.63
		285.27889	–	–	–	–	2.26
		298.07782	–	–	–	–	11.82
		299.08120	–	–	$[C_{24}H_{11}]^{rad+}$	–	2.20
		300.09340	300.09335	0.17	$[C_{24}H_{12}]^{rad+}$	2.4×10^8	100
		301.09681	301.09671	0.33	$[^{13}C\text{-}C_{23}H_{12}]^{rad+}$	5.0×10^7	2.08
		301.10121	301.10118	0.10	$[C_{24}H_{12}+H]^{rad+}$	1.6×10^8	66.7
		302.10016	302.10006	0.33	$[^{13}C_2\text{-}C_{22}H_{12}]^{rad+}$	6.7×10^6	2.79
		302.10461	302.10454	0.23	$[^{13}C\text{-}C_{23}H_{12}+H]^{+}$	3.9×10^7	16.3
		303.10346	303.10342	0.13	$[^{13}C_3\text{-}C_{21}H_{12}]^{rad+}$	5.9×10^5	0.24
		303.10800	303.10789	0.36	$[^{13}C_2\text{-}C_{22}H_{12}+H]^{+}$	5.6×10^6	2.34
		304.11134	304.11124	0.33	$[^{13}C_3\text{-}C_{21}H_{12}+H]^{+}$	5.8×10^5	0.24
		314.10468	–	–	–	6.1×10^5	0.25
		315.11247	–	–	–	4.2×10^5	0.17
		316.08845	316.08827	0.57	$[C_{24}H_{12}+O]^{rad+}$	1.2×10^6	0.50
		317.09635	317.09609	0.82	$[(C_{24}H_{12}+H)+O]^{+}$	2.8×10^6	1.17
	N_2	211.97856	–	–	–	–	12.1
		228.09369	–	–	–	–	9.37
		236.12849	–	–	–	–	26.4
		248.15051	–	–	–	–	3.53
		258.22544	–	–	–	–	5.93
		272.24115	–	–	–	–	8.03
		279.15959	–	–	–	–	6.15
		284.24115	–	–	–	–	3.68
		298.07829	–	–	–	–	6.19
		299.08162	–	–	$[C_{24}H_{11}]^{rad+}$	–	2.70
		300.09395	300.09335	2.00	$[C_{24}H_{12}]^{rad+}$	8.6×10^7	100
		301.09729	301.09671	1.93	$[^{13}C\text{-}C_{23}H_{12}]^{rad+}$	3.2×10^7	37.2
		301.10179	301.10118	2.03	$[C_{24}H_{12}+H]^{rad+}$	8.3×10^7	96.5
		302.10064	302.10006	1.92	$[^{13}C_2\text{-}C_{22}H_{12}]^{rad+}$	3.9×10^6	4.53
		302.10511	302.10454	1.89	$[^{13}C\text{-}C_{23}H_{12}+H]^{+}$	3.2×10^7	37.2
		303.10243	303.10342	3.27	$[^{13}C_3\text{-}C_{21}H_{12}]^{rad+}$	7.6×10^5	0.88
		303.10845	303.10789	1.85	$[^{13}C_2\text{-}C_{22}H_{12}+H]^{+}$	4.4×10^6	5.12
		304.12279	–	–	–	1.1×10^6	1.28
		314.09703	314.09643	1.91	$[C_{24}H_{12}+N]^{rad+}$	9.1×10^5	1.06
		315.10491	315.10425	2.09	$[(C_{24}H_{12}+H)+N]^{+}$	5.5×10^5	0.64
		316.08893	316.08827	2.09	$[C_{24}H_{12}+O]^{rad+}$	1.2×10^6	1.40
		317.09673	317.09609	2.02	$[(C_{24}H_{12}+H)+O]^{+}$	1.9×10^6	2.21
	He	211.97835	–	–	–	–	0.83
		228.09344	–	–	–	–	1.04
		236.12819	–	–	–	–	0.46
		257.24760	–	–	–	–	0.40
		277.10124	–	–	–	–	2.08
		285.27888	–	–	–	–	0.37
		298.07782	–	–	–	–	6.48
		299.08120	–	–	$[C_{24}H_{11}]^{rad+}$	–	1.50
		300.09339	300.09335	0.13	$[C_{24}H_{12}]^{rad+}$	1.6×10^8	84.2
		301.09684	301.09671	0.43	$[^{13}C\text{-}C_{23}H_{12}]^{rad+}$	2.9×10^7	15.3
		301.10119	301.10118	0.03	$[C_{24}H_{12}+H]^{rad+}$	1.9×10^8	100
		302.10015	302.10006	0.30	$[^{13}C_2\text{-}C_{22}H_{12}]^{rad+}$	2.9×10^6	1.53
		302.10462	302.10454	0.26	$[^{13}C\text{-}C_{23}H_{12}+H]^{+}$	3.3×10^7	17.4
		303.08049	303.10342	–	–	1.6×10^6	0.84
		303.10794	303.10789	0.16	$[^{13}C_2\text{-}C_{22}H_{12}+H]^{+}$	3.6×10^6	1.89
		304.11130	304.11124	0.20	$[^{13}C_3\text{-}C_{21}H_{12}+H]^{+}$	4.4×10^5	0.25
		314.09653	314.09643	0.32	$[C_{24}H_{12}+N]^{rad+}$	4.7×10^5	0.24
		315.11701	315.10425	–	–	1.6×10^6	0.84
		316.08838	316.08827	0.35	$[C_{24}H_{12}+O]^{rad+}$	5.0×10^5	0.26
		317.09635	317.09609	0.82	$[(C_{24}H_{12}+H)+O]^{+}$	1.3×10^6	0.68

in comparison with N_2. This behavior appears to be associated with the easy ionization of O_2 (EI: 12.1 eV). We can also attribute this behavior to the high electronegativity and oxidizing power of O_2, which can explain the use of low corona discharge values in the ionization of CAs (Table 1S). Conversely, although He is less reactive, it has a high ionization potential (24.6 eV) and a high expansion volume (sound velocity = 972 m s^{-1} and 20 °C). Consequently, the formation of its metastable state (He*) is energetically and kinetically favored in the ionization of solvent molecules, thus making the ionization of HCs and CAs more efficient. In the literature, this excess energy has been

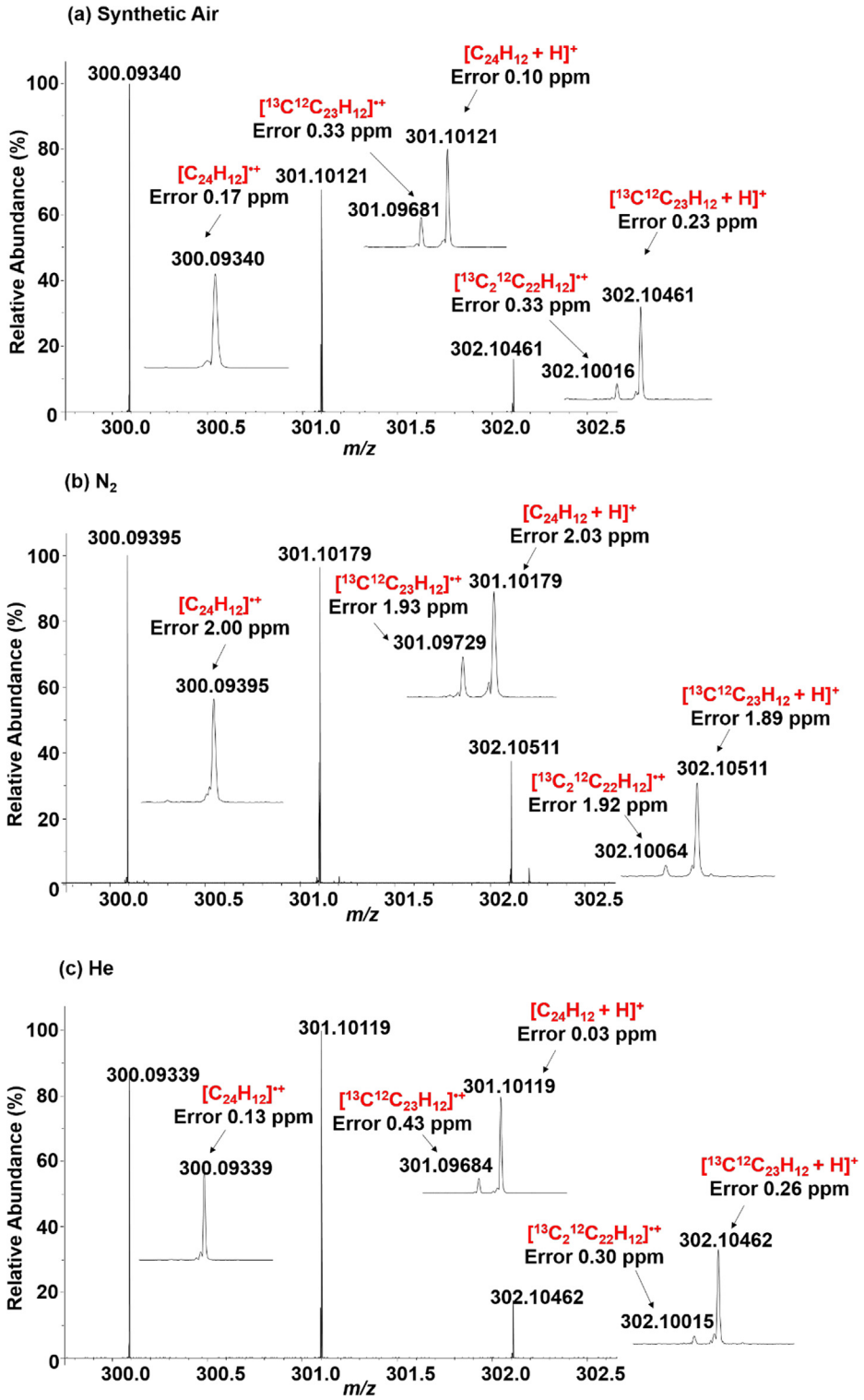

Fig. 5. Expanded insert of the *m/z* 300–303 region of the APCI(+) mass spectra (Fig. 4) of coronene using three ion source gases: synthetic air (a), N_2, (b), and He (c).

associated with the possible fragmentation of $[M\text{-alkyl}]^+$, where M = HC [19]. However, for the CA and HC standards, a reduction of fragmentation products and oxidative species was observed when He was used as a gas nebulizer. The increase in TIC and its signal-to-noise ratio proves the greater ionizing power of He compared with the other gases studied.

Tables 1 and 3 and S2–S5 summarize the molecular formulas of the detected ions, the theoretical and experimental *m/z*, the mass accuracy (in ppm), and the absolute values and percentage of the TIC of HC and CA standards as a function of the type applied ion source gas. In all cases, the nitrogenated and oxygenated species of $[(M+H)+O_x]^+$, $[(M+H)+N_y]^+$, $[(M-H)+O_x]^+$, $[(M-H)+N_y]^+$, $[M+O_x]^{\cdot+}$, and [M

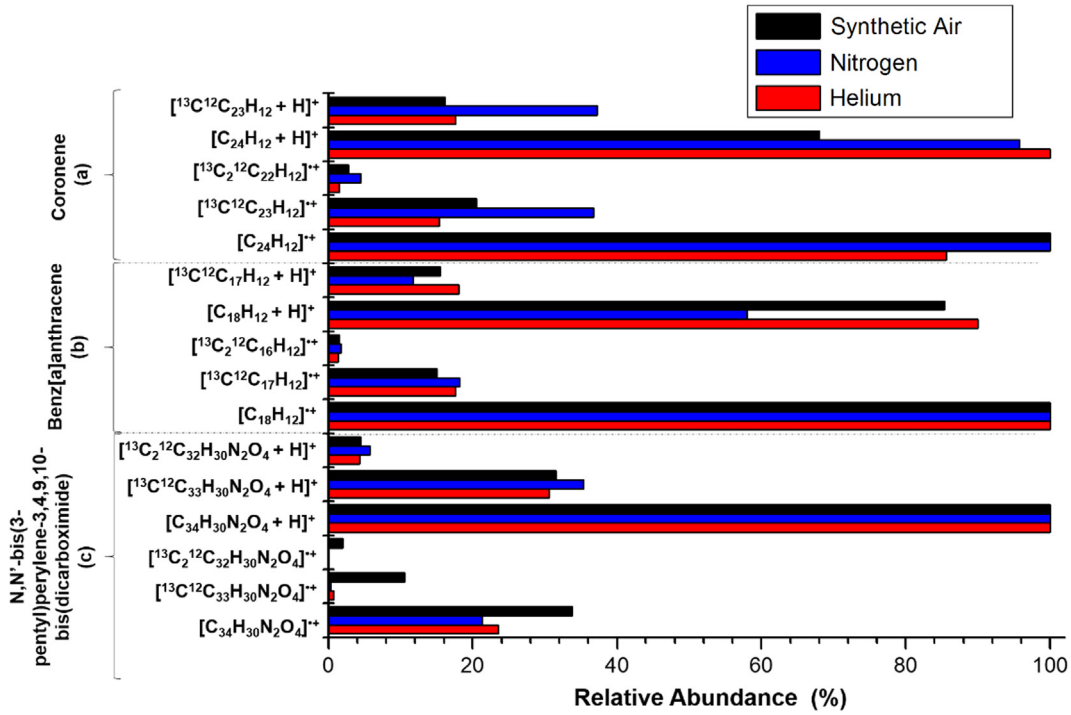

Fig. 6. Relative abundance of the isotopologue profile (M, M + 1, and M + 2) of ($M^{\cdot +}$) and $[M+H]^+$ species of CA standards with different types of ion source gases: (a) coronene, (b) benz[a]anthracene, and (c) N,N′-bis(3-pentyl)perylene-3,4,9,10-bis(dicarboximide).

$+N_y]^{\cdot +}$ were identified. Nyadong et al. [25] examined saturated HCs and detected the formation of oxygenated species. These authors suggested that these species could be formed because of the humidity present in the environment. Conversely, Jin et al. [23] found no obvious correlation between humidity and the adduction formation.

Note that oxygenated and nitrogenated molecules were formed in all the three types of ion source gases used in this study. This occurrence could be attributed to the artifact of the ionization conditions of the APCI(+) source, where the corona discharge caused a reaction among the drying gas (N_2), the isooctane, and the O_2 gas (atmosphere) originating from the formation of the protonated heteroatomic species [25]. However, the intensities of these species were different for each ionizing gas used (Tables 1, 3, and 2S–5S). For He, these species appeared in a low intensity whereas for synthetic air and N_2, the abundance of $[(M+H)+O_x]^+$, $[(M+H)+N_y]^+$, $[(M-H)+O_x]^+$, $[(M-H)+N_y]^+$, $[M+O_x]^{\cdot +}$ or $[M+N_y]^{\cdot +}$ ions was greater.

3.4. Paraffin analysis

The effect of the ionizing gas at the APCI(+) source was also tested to evaluate the ionization efficiency of the three paraffin samples (one analytical standard and two saturated fractions, SA_1 and SA_2). Fig. 7a–c illustrate the APCI(+)FT-ICR mass spectra for the synthetic paraffin standard. The MS spectra showed broad profiles at *m/z* 200–1400, with M_w values centered at approximately 808, 785, and 739 Da for synthetic air, N_2, and He, respectively. The paraffin standard is composed of a mixture of saturated HCs containing a bimodal Gaussian profile, which is formed by two CN distributions of C_5–C_{28} and C_{30}–C_{120}. The detected signals were attributed to the $[M-H]^+$ species. Aside from the two Gaussian distribution, a third was detected overlapping the signals of HCs at C_{30}–C_{120} in the region of *m/z* 450–1200. The distribution was composed of HC molecules attached to O_2 or N_2 atoms, such as the $[C_{48}H_{98}O\text{-}H]^+$ species with DBE = 0 and *m/z* 689.7554. A similar behavior was observed in the CA standards [22,24]. These species can be better represented as the $[(C_{48}H_{98}\text{-}H)+O]^+$ cation. This result explains the presence of the O_1 and O_2 classes in the class diagram (Fig. 7d) when using synthetic air or N_2 as the ionizing gas.

A DBE of zero represents the linear saturated HC molecule, that is, *n*-paraffins, branched, or iso-paraffins. Cycloparaffins may also be present in the saturated HC fractions extracted from crude oil, but these compounds have DBE > 0.

The DBE versus CN plots (Fig. 7e) of paraffin standard (C_5-C_{120}) show DBEs with majority values between 0 and 2. These DBEs indicated that the saturated and cyclic HCs were ionized. Synthetic air and He preferentially ionized molecules with CN of C_5–C_{95}, and N_2 ionized HCs with CN of C_{10}–C_{75}.

The APCI(+) mass spectra for the fraction SA_1 showed broad profiles of *m/z* 200–1600 for synthetic air and *m/z* 200–1400 for N_2 and He (Fig. 8a–c). The M_w values were 817, 699, and 673 Da, respectively, indicating the increase in M_w in the following order: He < N_2 < synthetic air. The class diagram of fraction SA_1 (Fig. 8d) revealed that the HCs were ionized preferentially by electron transfer ($M^{\cdot +}$) and transformed into heteroatomic classes (NO_2 and O_2) only when N_2 was used. The HC[H] class, represented by the $[M-H]^+$ species, were more abundant in the presence of He and synthetic air (Fig. 8d). The DBE versus CN plot for the HC[H] class of fraction SA_1 (Fig. 8a, b) showed a similar DBE distribution for all studied ionization gases (DBE: 2–16 for synthetic air, DBE: 3–15 for N_2, and DBE: 2–16 for He), as illustrated in Fig. 8f. As observed previously in the results of synthetic air and He (Fig. 7e), a larger amplitude of CN distribution of C_{15}–C_{95} was clearly observed in the DBE versus CN plot in relation to N_2 (C_{20}–C_{85}) (Fig. 8a–c). A similar result was found for fraction SA_2 (Fig. 9S).

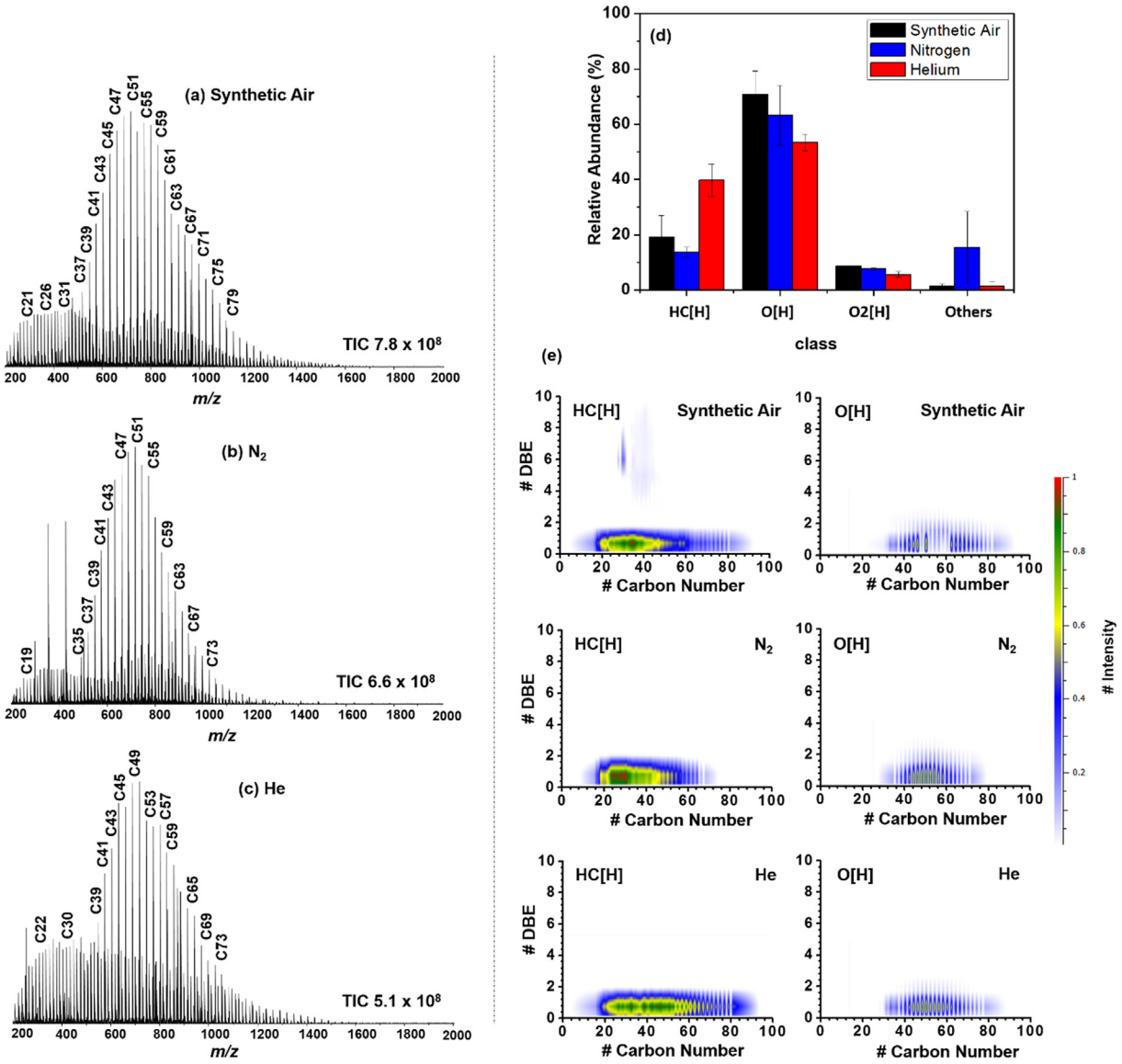

Fig. 7. FT-ICR mass spectra of the synthetic paraffin standard using three different ionizing gases at the APCI(+) source: (a) synthetic air, (b) N_2, (c) He, (d) class diagram and, (e) DBE vs. CN plots for HC[H] and O[H] classes as a function of the type of ion source gas.

4. Conclusion

The ionization of HC, CA, and paraffin standards was studied by APCI(+)FT-ICR MS using synthetic air, N_2, and He as ionizing gases. Three ionization mechanisms were observed: electron transfer ($M^{+\cdot}$), proton transfer ($[M+H]^+$), and hydride abstraction ($[M-H]^+$). In the ionization of HC standards, synthetic air and He presented better ionization efficiency than N_2, thus producing mass spectra with higher mass accuracy and signal-noise rate. Moreover, linear HCs were preferentially ionized through hydride abstraction (production of $[M-H]^+$ ions), observed in the hexatriacontane molecule for example. In the most cases, the ionization of unsaturated and cyclic HCs mostly generated $[M+H]^+$ and $[M^{\cdot +}]$ ions. The unique exception is related to the 5-α-cholestane molecule, which is ionized as $[M-H]^+$ in the presence of synthetic air. In evaluating the effect of ion source gases on the CA standards, N_2 and synthetic air mainly promoted the detection of CA standards through the electron transfer ($M^{+\cdot}$) mechanism, and He favored the ionization by proton transfer ($[M+H]^+$) with minimal fragmentation or oxidation of the analyte. Surprisingly, synthetic air showed an excellent signal-to-noise rate and a lower matrix suppression. For the *n*-paraffin samples, synthetic air and He presented similar ionization performance through hydride abstraction ($[M-H]^+$). These results show how complex is the study about the chemical composition of paraffins, which reflects in the crude oil industry as deposition problems. Therefore, the characterization of the paraffinic fractions will enable the crude oil industry to better know its composition and assist in the search of solutions to the problems caused by the deposition process.

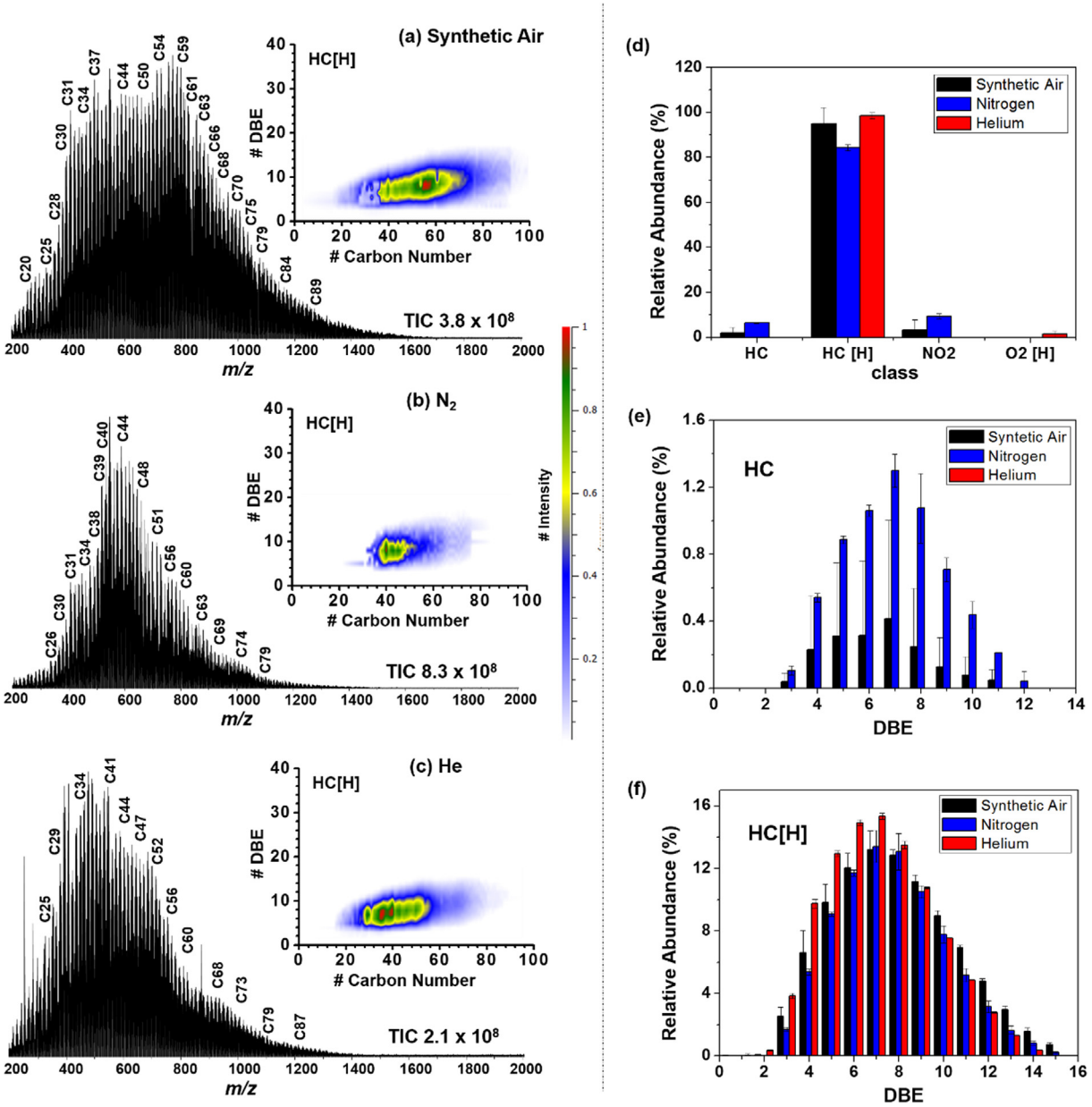

Fig. 8. FT-ICR mass spectra of the paraffin fraction SA1 using three different ion source gases at the APCI(+) source: (a) synthetic air, (b) N_2, (c) He, (d) class diagram and DBE vs. intensity plots for HC, and (e), (f) HC[H] classes in the function of the type of ionizing gas.

Acknowledgments

The authors are grateful to CAPES (23038.007083/2014-40), FAPES (734/2016), and CENPES/PETROBRAS for funding the research (process n. 2014/00254-5). The authors would also like to thank the Núcleo de Competências em Química do Petróleo for using their installations.

Appendix A. Supplementary data

Supplementary data associated with this article can be found, in the online version, at http://dx.doi.org/10.1016/j.fuel.2018.03.180.

References

[1] Pereira TM, Vanini G, Tose LV, Cardoso FM, Fleming FP, Rosa PT, et al. FT-ICR MS analysis of asphaltenes: asphaltenes go in, fullerenes come out. Fuel 2014;131:49–58.

[2] Pereira TM, Vanini G, Oliveira EC, Cardoso FM, Fleming FP, Neto AC, et al. An evaluation of the aromaticity of asphaltenes using atmospheric pressure photoionization Fourier transform ion cyclotron resonance mass spectrometry–APPI (±) FT-ICR MS. Fuel 2014;118:348–57.

[3] Barros EV, Dias HP, Gomes AO, Rodrigues RR, Moura RR, Sad CM, et al. Study of degradation of acid crude oil by high resolution analytical techniques. J Petrol Sci Eng 2017;154:194–203.

[4] Klein GC, Angström A, Rodgers RP, Marshall AG. Use of saturates/aromatics/resins/asphaltenes (SARA) fractionation to determine matrix effects in crude oil analysis by electrospray ionization Fourier transform ion cyclotron resonance mass spectrometry. Energy Fuel 2006;20:668–72.

[5] Terra LA, Filgueiras PR, Tose LV, Romao W, de Souza DD, de Castro EV, et al. Petroleomics by electrospray ionization FT-ICR mass spectrometry coupled to partial least squares with variable selection methods: prediction of the total acid number of crude oils. Analyst 2014;139:4908–16.

[6] Vaz BG, Abdelnur PV, Rocha WF, Gomes AO, Pereira RC. Predictive petroleomics: measurement of the total acid number by electrospray Fourier transform mass spectrometry and chemometric analysis. Energy Fuel 2013;27:1873–80.

[7] Marshall AG, Rodgers RP. Petroleomics: the next grand challenge for chemical analysis. Acc Chem Res 2004;37:53–9.

[8] Comisarow MB, Marshall AG. Frequency-sweep Fourier transform ion cyclotron resonance spectroscopy. Chem Phys Lett 1974;26:489–90.

[9] Lorente E, Berrueco C, Herod AA, Millan M, Kandiyoti R. The detection of high-mass

aliphatics in petroleum by matrix-assisted laser desorption/ionisation mass spectrometry. Rapid Commun Mass Spectrom 2012;26:1581–90.
[10] Pantoja PA, Mendes MA, Nascimento CAO. Contribution of mass spectrometry in assessing quality of petroleum fractions: the use of mass spectrometry for assessing asphaltenes. J Petrol Sci Eng 2013;109:198–205.
[11] Pinto FE, Silva CF, Tose LV, Figueiredo MA, Souza WC, Vaz BG, et al. Evaluation of adsorbent materials for the removal of nitrogen compounds in vacuum gas oil by positive and negative electrospray ionization Fourier transform ion cyclotron resonance mass spectrometry. Energy Fuel 2017;31:3454–64.
[12] Dias HP, Dixini PV, Almeida LC, Vanini G, Castro EV, Aquije GM, et al. Evidencing the crude oil corrosion by Raman spectroscopy, atomic force microscopy and electrospray ionization FT-ICR mass spectrometry. Fuel 2015;139:328–36.
[13] Liu Y, Kujawinski EB. Chemical composition and potential environmental impacts of water-soluble polar crude oil components inferred from ESI FT-ICR MS. PLoS One 2015;10:e0136376.
[14] Tose LV, Cardoso FM, Fleming FP, Vicente MA, Silva SR, Aquije GM, et al. Analyzes of hydrocarbons by atmosphere pressure chemical ionization FT-ICR mass spectrometry using isooctane as ionizing reagent. Fuel 2015;153:346–54.
[15] Hourani N, Kuhnert N. Development of a novel direct-infusion atmospheric pressure chemical ionization mass spectrometry method for the analysis of heavy hydrocarbons in light shredder waste. Anal Method 2012;4:730–5.
[16] Cho Y, Birdwell JE, Hur M, Lee J, Kim B, Kim S. Extension of the analytical window for characterizing aromatic compounds in oils using a comprehensive suite of high-resolution mass spectrometry techniques and double bond equivalence versus carbon number plot. Energy Fuels 2017;31(8):7874–83.
[17] Purcell JM, Hendrickson CL, Rodgers RP, Marshall AG. Atmospheric pressure photoionization Fourier transform ion cyclotron resonance mass spectrometry for complex mixture analysis. Anal Chem 2006;78:5906–12.
[18] Crawford KE, Campbell JL, Fiddler MN, Duan P, Qian K, Gorbaty ML, et al. Laser-induced acoustic desorption/Fourier transform ion cyclotron resonance mass spectrometry for petroleum distillate analysis. Anal Chem 2005;77:7916–23.
[19] Gao J, Borton DJ, Owen BC, Jin Z, Hurt M, Amundson LM, et al. Laser-induced acoustic desorption/atmospheric pressure chemical ionization mass spectrometry. J Am Soc Mass Spectrom 2011;22:531–8.
[20] Wu C, Qian K, Nefliu M, Cooks RG. Ambient analysis of saturated hydrocarbons using discharge-induced oxidation in desorption electrospray ionization. J Am Soc Mass Spectrom 2010;21:261–7.
[21] Houriet R, Parisod G, Gaumann T. The mechanism of chemical ionization of n-paraffins. J Am Chem Soc 1977;99:3599–602.
[22] Campbell JL, Crawford KE, Kenttämaa HI. Analysis of saturated hydrocarbons by using chemical ionization combined with laser-induced acoustic desorption/Fourier transform ion cyclotron resonance mass spectrometry. Anal Chem 2004;76:959–63.
[23] Jin C, Viidanoja J, Li M, Zhang Y, Ikonen E, Root A, et al. Comparison of atmospheric pressure chemical ionization and field ionization mass spectrometry for the analysis of large saturated hydrocarbons. Anal Chem 2016;88:10592–8.
[24] Gao J, Owen BC, Borton DJ, Jin Z, Kenttämaa HI. HPLC/APCI mass spectrometry of saturated and unsaturated hydrocarbons by using hydrocarbon solvents as the APCI reagent and HPLC mobile phase. J Am Soc Mass Spectrom 2012;23:816–22.
[25] Nyadong L, Quinn JP, Hsu CS, Hendrickson CL, Rodgers RP, Marshall AG. Atmospheric pressure laser-induced acoustic desorption chemical ionization mass spectrometry for analysis of saturated hydrocarbons. Anal Chem 2012;84:7131–7.
[26] Marotta E, Paradisi C. A mass spectrometry study of alkanes in air plasma at atmospheric pressure. J Am Soc Mass Spectrom 2009;20:697–707.
[27] Hourani N, Muller H, Adam FM, Panda SK, Witt M, Al-Hajji AA, et al. Structural level characterization of base oils using advanced analytical techniques. Energy Fuel 2015;29:2962–70.
[28] Horning EC, Horning MG, Carroll DI, Dzidic I, Stillwell RN. New picogram detection system based on a mass spectrometer with an external ionization source at atmospheric pressure. Anal Chem 1973;45:936–43.
[29] De Hoffmann E, Stroobant V. Mass spectrometry: principles and applications. third ed. England: John Wiley & Sons; 2007.
[30] Yoshimura K, Przybilla L, Ito S, Brand JD, Wehmeir M, Räder HJ, et al. Characterization of large synthetic polycyclic aromatic hydrocarbons by MALDI- and LD-TOF mass spectrometry. Macromol Chem Phys 2001;202(2):215–22.
[31] Ghislain T, Faure P, Michels R. Detection and monitoring of PAH and Oxy-PAHs by high resolution mass spectrometry: comparison of ESI, APCI and APPI source detection. J Am Soc Mass Spectrom 2012;23:530–6.
[32] Owen BC, Gao J, Borton DJ, Amundson LM, Archibold EF, Tan X, et al. Carbon disulfide reagent allows the characterization of nonpolar analytes by atmospheric pressure chemical ionization mass spectrometry. Rapid Commun Mass Spectrom 2011;25(14):1924–8.
[33] Aue DH, Guidoni M, Betowski LD. Ab initio calculated gas-phase basics of polynuclear aromatic hydrocarbons. Int J Mass Spectrom 2000;201:283–95.